Rotationally resolved photoelectron spectra in resonance enhanced multiphoton ionization of HCl via the F 1Δ2 Rydberg state

Kwanghsi Wang and V. McKoy

Citation: The Journal of Chemical Physics **95**, 8718 (1991); doi: 10.1063/1.461256
View online: http://dx.doi.org/10.1063/1.461256
View Table of Contents: http://scitation.aip.org/content/aip/journal/jcp/95/12?ver=pdfcov
Published by the AIP Publishing

Rotationally resolved photoelectron spectra in resonance enhanced multiphoton ionization of HCl via the $F\,^1\Delta_2$ Rydberg state

Kwanghsi Wang and V. McKoy
Arthur Amos Noyes Laboratory of Chemical Physics,[a] California Institute of Technology, Pasadena, California 91125

(Received 27 August 1991; accepted 13 September 1991)

Results of studies of rotational ion distributions in the $X\,^2\Pi_{3/2}$ and $X\,^2\Pi_{1/2}$ spin-orbit states of HCl^+ resulting from $(2+1')$ resonance enhanced multiphoton ionization (REMPI) via the $S(0)$ branch of the $F\,^1\Delta_2$ Rydberg state are reported and compared with measured threshold-field-ionization zero-kinetic-energy spectra reported recently [K. S. Haber, Y. Jiang, G. Bryant, H. Lefebvre-Brion, and E. R. Grant, Phys. Rev. A (in press)]. These results show comparable intensities for $J^+ = 3/2$ of the $X\,^2\Pi_{3/2}$ ion and $J^+ = 1/2$ of the $X\,^2\Pi_{1/2}$ ion. Both transitions require an angular momentum change of $\Delta N = -1$ upon photoionization. To provide further insight into the near-threshold dynamics of this process, we also show rotationally resolved photoelectron angular distributions, alignment of the ion rotational levels, and rotational distributions for the parity components of the ion rotational levels. About 18% population is predicted to occur in the $(+)$ parity component, which would arise from odd partial-wave contributions to the photoelectron matrix element. This behavior is similar to that in $(2+1)$ REMPI via the $S(2)$ branch of the $F\,^1\Delta_2$ state of HBr and was shown to arise from significant l mixing in the electronic continuum due to the nonspherical molecular ion potential. Rotational ion distributions resulting from $(2+1)$ REMPI via the $S(10)$ branch of the $F\,^1\Delta_2$ state are also shown.

I. INTRODUCTION

Resonance enhanced multiphoton ionization (REMPI) coupled with high-resolution photoelectron spectroscopy has become an important tool for probing the characteristics of excited electronic states and their photoionization dynamics.[1-3] With REMPI, a single rotational level of the resonant intermediate state is selected and therefore only a few rotational levels of the ion are formed. This results in substantial simplifications in the photoelectron spectra. Such rotationally resolved REMPI photoelectron spectra are usually studied using time-of-flight measurements[4-8] for molecules with larger rotational spacings. Recently, Müller-Dethlefs, Sander, and Schlag[9] and Sander *et al.*[10] have further achieved an energy resolution of less than 1 cm^{-1} using the zero-kinetic-energy (ZEKE) technique. This technique provides a new tool for investigating the dynamics of near-threshold photoionization[11,12] and is particularly useful in exploring excited states with small rotational constants. Of specific interest to the present studies are the rotational distribution of HCl^+ ions resulting from $(2+1')$ REMPI of HCl via the $S(0)$ branch of the $F\,^1\Delta_2(4p\pi)$ state.[12] These threshold-field-ionization zero-kinetic-energy spectra show comparable intensities for $J^+ = 3/2$ of the $X\,^2\Pi_{3/2}$ ion and $J^+ = 1/2$ of the $X\,^2\Pi_{1/2}$ ion. Both transitions require an angular momentum change of $\Delta N = N^+ - N' = -1$ upon photoionization, with N^+ and N' the rotational quantum numbers of the ionic and intermediate states, respectively.

Recently, Xie and Zare[13,14] have used laser-induced fluorescence (LIF) to measure the rotational ion distributions resulting from $(2+1)$ REMPI of HBr via the $S(2)$ branch of the $F\,^1\Delta_2(5p\pi)$ Rydberg state. Interesting features of these rotational ion distributions included (i) a pronounced $\Delta N = 0$ peak in the $X\,^2\Pi_{1/2}$ spin-orbit state, (ii) a strongly $(-)$ parity-favored distribution expected on the basis of the dominant (even) partial-wave components of the photoelectron matrix element, (iii) 20% population in the $(+)$ parity component which would have to arise from odd partial-wave contributions to the photoelectron matrix element, and (iv) no ions in the $X\,^2\Pi_{3/2}$ spin-orbit state. In recent studies Wang and McKoy[15] have successfully accounted for the significant features seen in these measured rotational ion spectra.

In this paper we present results of studies of the "ZEKE" rotational ion distributions resulting from $(2+1')$ REMPI via the $S(0)$ branch of the $F\,^1\Delta_2$ Rydberg state of HCl. The calculated and measured spectra both show the $J^+ = 1/2$ peak to be the most intense for the $X\,^2\Pi_{1/2}$ ionic state. This transition, in turn, requires a rotational angular momentum change of $\Delta N = -1$, which differs from the $\Delta N = 0$ expected for higher J transitions. To provide further insight into the underlying dynamics of this near-threshold REMPI process, rotational ion distributions for the parity components of the Λ doublet of the ion rotational levels and associated photoelectron angular distributions are also presented. In addition to the dominant population seen in the $(-)$ parity component of the J^+ levels, about 18% population is predicted to occur in the other parity component. This $(+)$ parity component would have to arise from odd partial-wave contributions to the photoelectron matrix element. This behavior is similar to that seen in $(2+1)$ REMPI via the $S(2)$ branch of the $F\,^1\Delta_2$ state of HBr.[13-15] The calculated alignment of individual ion rota-

[a] Contribution No. 8498.

 0021-9606/91/248718-07$03.00

tional levels shows that a significant change in alignment occurs upon photoionization. Rotationally resolved photoelectron angular distributions which provide significant insight into the underlying photoionization dynamics are also shown. Several differences between the photoelectron spectra of HCl and HBr are found and discussed. Rotational ion distributions resulting from (2 + 1) REMPI of HCl via the $S(10)$ branch of the $F\,^1\Delta_2$ state are also presented.

II. THEORY AND CALCULATION

A. Differential cross section

The (2 + 1′) REMPI processes via the S branch of the $F\,^1\Delta_2(4p\pi)$ intermediate Rydberg state of HCl can be summarized as

$$\mathrm{HCl}[X\,^1\Sigma^+(v_0=0,J_0,e)] \xrightarrow{2\omega} \mathrm{HCl}^*[F\,^1\Delta(v=0,J=N=J_0+2,e)] \xrightarrow{\omega'} \mathrm{HCl}^+[X\,^2\Pi(v^+=0,J^+,N^+,e,f)]+e^-(\mathbf{k}), \quad (1)$$

where e/f designates parity.[16] For linearly polarized light, ionization originating from each of the $(2J_0+1)$ magnetic sublevels of the initial state forms an independent channel. The rotationally resolved differential cross section for ionization out of the M_J levels of the resonant intermediate state can be expressed in terms of Legendre polynomials as

$$\frac{d\sigma}{d\Omega} \propto \sum_{M_J M_{J^+}} \rho_{M_J M_J} |\Gamma_{M_J M_{J^+}}|^2 = \frac{\sigma}{4\pi}\left[1+\sum_{L=1}^{L_{\max}} \beta_{2L} P_{2L}(\cos\theta)\right], \quad (2)$$

where σ is the total cross section; β_n, the asymmetry parameters; $P_l(\cos\theta)$, Legendre polynomials; and $L_{\max}=3$. In Eq. (2), $\rho_{M_J M_J}$ is the population of a specific M_J level of the resonant intermediate state created by two-photon excitation. For the $S(J_0)$ branch of interest here, $\rho_{M_J M_J}$ has the simple form

$$\rho_{M_J M_J} = \mathcal{N}(J_0+M_J+1)(J_0+M_J+2) \times (J_0-M_J-1)(J_0-M_J-2), \quad (3)$$

where $\mathcal{N}$ is a normalization constant. In the simplest case of $J_0=0$, $\rho_{M_J M_J}=\delta_{M_J,0}$ with δ_{ij} the Kronecker delta function. $|\Gamma_{M_J M_{J^+}}|^2$ of Eq. (2) is the probability for photoionization of the M_J level of the intermediate state leading to the M_{J^+} level of the ionic state. A formula for $\Gamma_{M_J M_{J^+}}$ has been derived by Wang and McKoy[17] by explicitly considering the spin coupling associated with multiplet-specific final-state wave functions and intermediate coupling schemes between Hund's cases (a) and (b) for describing the resonant and ionic states.

Parity selection rules,[17–20] governing changes of rotational angular momentum upon photoionization, have been previously derived and are of the form

$$\Delta J + \Delta S + \Delta p + l = \text{even}, \quad (4)$$

where $\Delta J = J^+ - J$, $\Delta S = S^+ - S$, $\Delta p = p^+ - p$. In Eq. (4), J denotes the total angular momentum, S the total spin, l a partial-wave component of the photoelectron, and p the parity index, i.e., 0 for e states and 1 for f states. In the Hund's case (b) limit, Eq. (4) further reduces to $\Delta N + \Delta p + l = \text{odd}$.[17–20]

B. Multiplet-specific wave functions and potentials

There are three dipole-allowed transition channels for photoionization of the $3\pi(4p\pi)$ orbital of the resonant $F\,^1\Delta_2$ Rydberg state. The corresponding multiplet-specific final-state wave functions are given by

$$\Psi(^1\Pi) = (1/\sqrt{2})\left[|(\text{core})2\pi_+^2\, 2\pi_-\, \overline{k\sigma}| - |(\text{core})2\pi_+^2\, \overline{2\pi}_-\, k\sigma|\right], \quad (5a)$$

$$\Psi(^1\Delta) = (1/\sqrt{2})\left[|(\text{core})2\pi_+^2\, 2\pi_-\, \overline{k\pi}_+| - |(\text{core})2\pi_+^2\, \overline{2\pi}_-\, k\pi_+|\right], \quad (5b)$$

and

$$\Psi(^1\Phi) = (1/\sqrt{2})\left[|(\text{core})2\pi_+^2\, 2\pi_-\, \overline{k\delta}_+| - |(\text{core})2\pi_+^2\, \overline{2\pi}_-\, k\delta_+|\right], \quad (5c)$$

with $(\text{core}) = 1\sigma^2 2\sigma^2 3\sigma^2 4\sigma^2 5\sigma^2 1\pi^4$.

Within the frozen-core Hartree–Fock approximations, the one-particle Schrödinger equation for the photoelectron orbital ϕ_k can be shown to have the form[21,22]

$$P\Big(f+\sum_{i=\text{core}}(2J_i-K_i)+a_n J_n+b_n K_n + \alpha S''_{2\pi}+\beta S'_{2\pi}-\epsilon\Big)P|\phi_k\rangle = 0, \quad (6)$$

where J_i and K_i are the Coulomb and exchange operators, respectively, and P is a projection operator which enforces orthogonality of the continuum orbital to the occupied orbitals.[21,22] The photoelectron kinetic energy is given by $\epsilon = (1/2)k^2$. The operators S'' and S' are defined by

$$S''_\pi \phi_+(\mathbf{r}_1) = \phi_-(\mathbf{r}_1)\int d^3\mathbf{r}_2[\pi_-(\mathbf{r}_2)^*]\frac{1}{r_{12}}\pi_+(\mathbf{r}_2), \quad (7)$$

and

$$S'_\pi \phi_+(\mathbf{r}_1) = \pi_+(\mathbf{r}_1)\int d^3\mathbf{r}_2[\pi_-(\mathbf{r}_2)]^*\frac{1}{r_{12}}\phi_-(\mathbf{r}_2). \quad (8)$$

The one-electron operator f in Eq. (6) is

$$f = -\frac{1}{2}\nabla_i^2 - \sum_\alpha \frac{Z_\alpha}{r_{i\alpha}}, \quad (9)$$

where Z_α is a nuclear charge. Using the wave functions of Eq. (5), the coefficients α, β, a_n, and b_n associated with the $2\pi_+$ orbital assume values of 0, 0, 2, and −1, respectively. The corresponding values for the $2\pi_-$ orbital are 0, 0, 2, and 1.

C. Numerical details

We used the improved virtual orbital method[23] to obtain the wave functions of the $F\,^1\Delta_2(2\pi\rightarrow 3\pi)$ resonant Rydberg state. The core orbitals are taken to be those of the fully

relaxed $^2\Pi(2\pi^{-1})$ ion. The orbital basis used in these calculations consists of a [6*s*,5*p*] contraction of the (12*s*,9*p*) primitive Cartesian Gaussian basis of Dunning,[24] augmented by one *s* ($\alpha = 0.1$) and two *d* ($\alpha = 0.68$ and 0.15) functions on the chlorine atom. On the hydrogen we use the [3*s*,1*p*] contraction of a (4*s*,2*p*) primitive Cartesian Gaussian basis of Dunning[25] augmented with one *s* ($\alpha = 0.1$) and two *p* ($\alpha = 0.25$ and 0.1) functions. This basis was augmented with four *s* and *p* ($\alpha = 0.05$, 0.02, 0.008, and 0.002) and three *d* ($\alpha = 0.055$, 0.015, and 0.005) functions at the center of mass (CM). With this basis set and choice of wave functions, we obtained a total energy of $-459.755\,055$ a.u. at $R_e = 2.484\ a_0$ for the $F\,^1\Delta_2$ Rydberg state.

To obtain the photoelectron orbitals we have used an iterative procedure, based on the Schwinger variational principle,[21,22] to solve the Lippmann–Schwinger equation associated with Eq. (6). In this procedure, the static-exchange potential is approximated by

$$U(\mathbf{r},\mathbf{r}') = \sum_{ij} \langle \mathbf{r}|U|\alpha_i\rangle (U^{-1})_{ij} \langle \alpha_j|U|\mathbf{r}'\rangle, \qquad (10)$$

where the matrix U^{-1} is the inverse of the matrix with elements $(U)_{ij} = \langle \alpha_i|U|\alpha_j\rangle$ and the α's are discrete basis functions such as Cartesian or spherical Gaussian functions. U is twice the static-exchange potential in Eq. (6) with the long-range Coulomb potential removed. The Lippmann–Schwinger equation with this separable potential $U(\mathbf{r},\mathbf{r}')$ can be readily solved providing approximate photoelectron orbitals $\phi_k^{(0)}$. These solutions can be iteratively improved to yield converged solutions to the Lippmann–Schwinger equation containing the full static-exchange potential. In this study, two iterations provided converged solutions of Eq. (6). The basis sets used in the separable expansion of Eq. (10) are listed in Table I.

TABLE I. Basis sets used in the separable potential of Eq. (10).

Symmetry	Center	Type of Gaussian function[a]	Exponents
σ	Cl	Cartesian *s*	8.0, 4.0, 2.0, 1.0, 0.5, 0.25
		z	2.0, 1.0, 0.5, 0.25, 0.1
	CM	Spherical $l = 0$–4	2.0, 1.0, 0.5
	H	Cartesian *s*	1.2, 0.4, 0.1
		z	1.2, 0.4, 0.1
π	Cl	Cartesian *x*	8.0, 4.0, 2.0, 1.0, 0.5, 0.25
		xz	2.0, 1.0, 0.5, 0.25, 0.1
	CM	Spherical $l = 1$–4	2.0, 1.0, 0.5
	H	Cartesian *x*	1.2, 0.4, 0.1
		xz	1.2, 0.4, 0.1
δ	Cl	Cartesian *xy*	8.0, 4.0, 2.0, 1.0, 0.5, 0.25, 0.1
	CM	Spherical $l = 2$–4	2.0, 0.75
	H	Cartesian *xy*	1.2, 0.4, 0.1

[a]Cartesian Gaussian basis functions are defined as $\phi^{\alpha,l,m,n,A}(\mathbf{r}) = \mathcal{N}(X-A_x)^l(y-A_y)^m(z-A_z)^n \exp(-\alpha|\mathbf{r}-\mathbf{A}|^2)$ and spherical Gaussian functions as $\phi^{\alpha,l,m,A}(\mathbf{r}) = \mathcal{N}|\mathbf{r}-\mathbf{A}|^l \times \exp(-\alpha|\mathbf{r}-\mathbf{A}|^2)\ Y_{lm}(\Omega_{\mathbf{r}-\mathbf{A}})$, with $\mathcal{N}$ the normalization constant.

All matrix elements arising in the solution of the Lippmann–Schwinger equation were evaluated via single-center expansions about the CM. For converged results, the following parameters were used:[21]

(i) Maximum partial wave of the photoelectron continuum orbital = 7.

(ii) Maximum partial-wave expansion of bound orbitals in the direct potential = 60.

(iii) Maximum partial-wave expansion of the 1σ, 2σ, 3σ, 4σ, 5σ, 1π, and 2π bound orbitals in the exchange potential = 30, 30, 25, 25, 20, 15, and 15, respectively.

(iv) Maximum partial-wave expansion of $1/r_{12}$ in the direct and exchange terms = 60 and 30, respectively.

(v) Maximum partial-wave expansion of the nuclear potential = 60.

The radial integration grid extends to 64 a.u. and contained 800 points. The integration step sizes ranged from 0.01 to 0.16 up to 16 a.u., and up to 0.16 a.u. beyond this point.

III. RESULTS AND DISCUSSION

A. (2+1′) REMPI via the $F\,^1\Delta_2$ Rydberg state

In Fig. 1 we compare calculated rotational ion distributions [Figs. 1(c) and 1(d)] resulting from (2 + 1′) REMPI of HCl via the $S(0)$ branch of the $F\,^1\Delta_2$ Rydberg state with the experimental data [Figs. 1(a) and 1(b)] of Haber *et al.*[12] The photoelectron kinetic energy used in the calculation is 50 meV. The agreement between the calculated and measured ion distributions is good. Both calculated and measured spectra show the most-intense peaks to be the $J^+ = 3/2$ level for the $X\,^2\Pi_{3/2}$ spin-orbit state and the $J^+ = 1/2$ level for the $X\,^2\Pi_{1/2}$ state. Both ionic states require an angular momentum change of $\Delta N = -1$ upon photoionization. This behavior is also predicted for the rotational branching ratios of HBr in (2 + 1′) REMPI via the $S(0)$ and $S(1)$ branches of the $F\,^1\Delta_2$ Rydberg state.[15] In the high-J limit, $\Delta N = 0$ transitions are expected to be most intense in both spin-orbit states. In Fig. 1, a sum over the (+) and (−) parity components of the J^+ rotational levels is assumed in the calculation. As expected from the parity-selection rule of Eq. (4), the (−) parity component of the J^+ rotational levels is predominantly populated via even partial-wave contributions to the photoelectron matrix element since the 3π orbital of the $F\,^1\Delta_2$ Rydberg state, at the R_e of 2.484 a.u., has 95.25% *p* and 4.70% *d* character in a single-center expansion around the CM. The calculated spectra are convoluted with a Gaussian detector function with a full-width at half-maximum (FWHM) of 5 cm^{-1}. In Fig. 2 we show rotationally resolved photoelectron angular distributions associated with the ion distributions of Fig. 1. These distributions reflect the angular momentum composition of the photoelectron matrix element. An incoherent sum over the (+) and (−) parity components of the Λ doublet of the J^+ rotational levels is assumed in evaluating the β parameters and hence both even and odd partial-wave components of the photoelectron matrix element contribute to these angular distributions. However, the even partial-wave contributions are expected to be dominant due to the almost pure *p* character of the $3\pi(4p\pi)$ orbital. The physical insight associated with these photoelectron angular distribu-

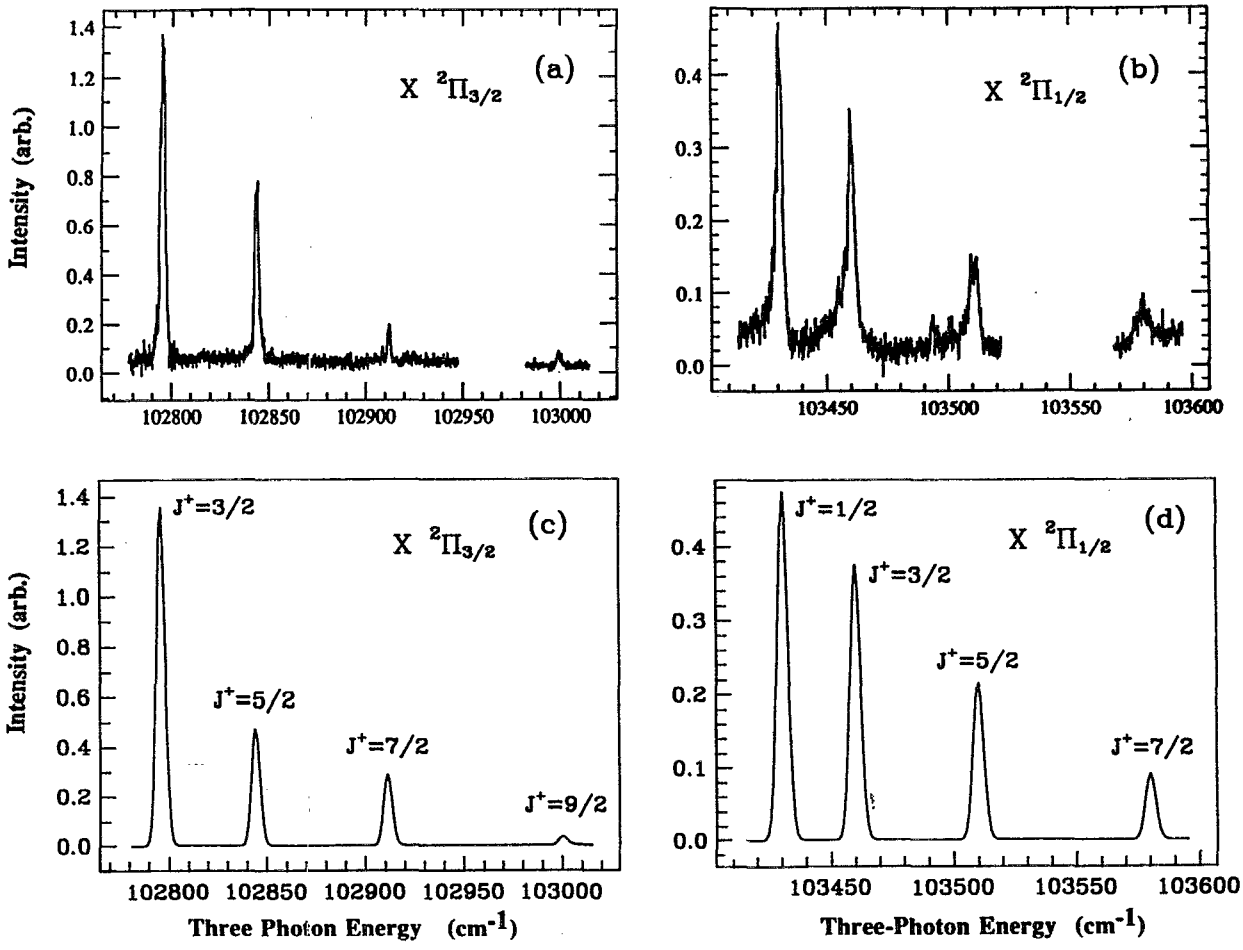

FIG. 1. Rotational ion distributions of measured [(a),(b)] and calculated [(c),(d)] photoelectron spectra resulting from (2 + 1′) REMPI of HCl via the $S(0)$ branch of the $F^1\Delta_2$ Rydberg state. A photoelectron energy of 50 meV is assumed in the calculation. The calculated spectra are convoluted with a Gaussian detector function with an FWHM of 5 cm^{-1} and summed over the (+) and (−) parity components.

tions for each parity component will be discussed later. Terms up to β_6 are included in Eq. (2).

Figure 3 shows the alignment predicted for the different J^+ levels of HCl^+ produced via the $S(0)$ branch of the $F^1\Delta_2$ state. These populations have been normalized to unity for each J^+ level. Again, this alignment contains contributions from both (+) and (−) parity components. These results show that a significant change in alignment occurs upon ionization. The alignment associated with the $\Delta J = -1/2$ photoionizing transitions (associated with $J^+ = 3/2$) is significantly different for the two spin-orbit states of the ion. For example, the $M_{J^+} = \pm 1/2$ sublevels

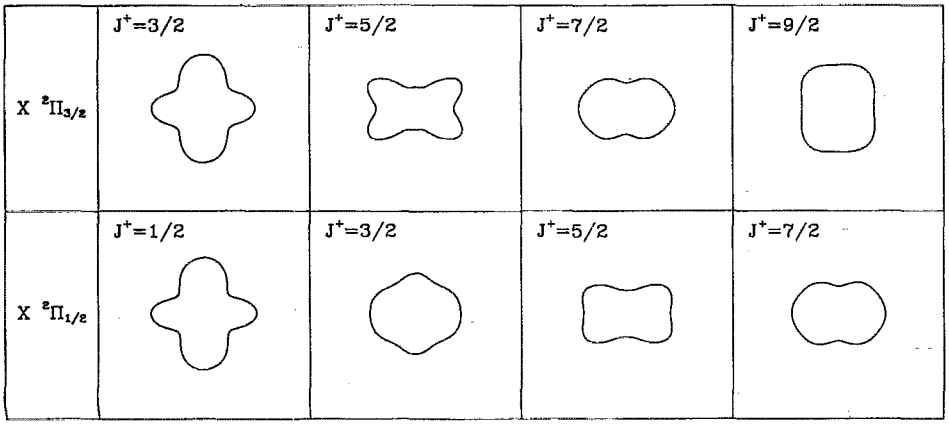

FIG. 2. Photoelectron angular distributions corresponding to the J^+ rotational levels of Fig. 1. An incoherent sum over the (+) and (−) parity components of the J^+ levels is assumed. 0° is vertical.

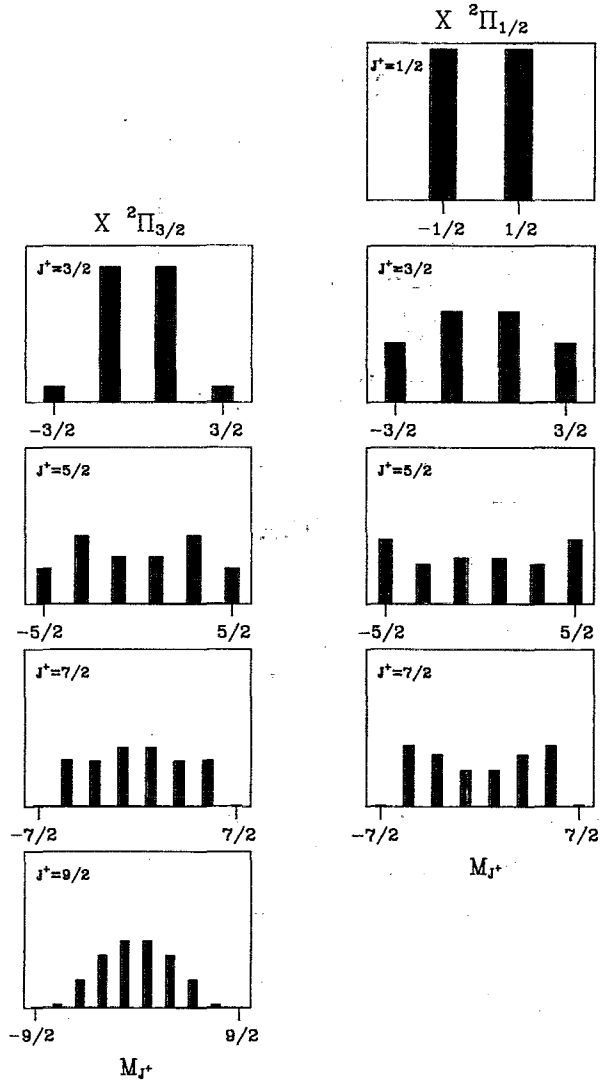

FIG. 3. Relative population (alignment) of the J^+ rotational levels via the $S(0)$ branch of the $F\,^1\Delta_2$ state. The population of each J^+ level is normalized to unity.

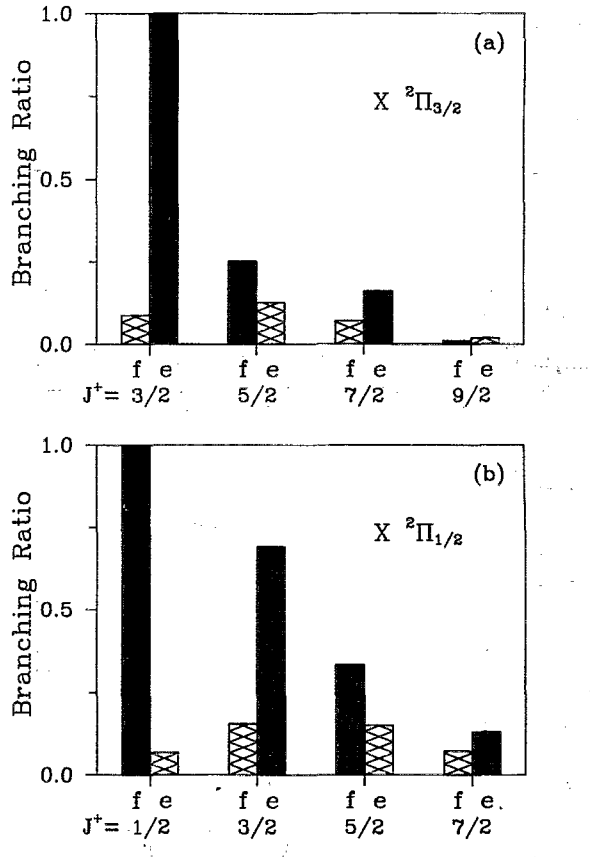

FIG. 4. Rotational ion distributions for the parity components of the J^+ rotational levels of Fig. 1 for (a) $X\,^2\Pi_{3/2}$ and (b) $X\,^2\Pi_{1/2}$ spin-orbit states. Solid and cross-hatched bars denote the (−) and (+) parity components, respectively.

are predicted to be dominant in the $X\,^2\Pi_{3/2}$ ($J^+ = 3/2$) spin-orbit state. However, an almost equal population is predicted for M_{J^+} sublevels of $J^+ = 3/2$ in the $X\,^2\Pi_{1/2}$ spin-orbit state.

Recently, Xie and Zare[13,14] have measured rotational ion distributions, deduced from LIF spectra, resulting from (2 + 1) REMPI of HBr via the $S(2)$ branch of the $F\,^1\Delta_2$ state. About 20% population is seen in the (+) parity component of the Λ doublet of the J^+ rotational levels. Population of this (+) parity component is due to odd partial-wave contributions to the photoelectron matrix elements. Theoretical analysis shows that this arises from the nonatomic-like behavior of the photoelectron continuum. To provide further insight into these near-threshold processes and to compare with the results of the studies of HBr, we show rotational ion distributions for the parity components of the Λ doublet of the ionic rotational levels in Fig. 4. As expected from the parity-selection rule of Eq. (4), population is fa-

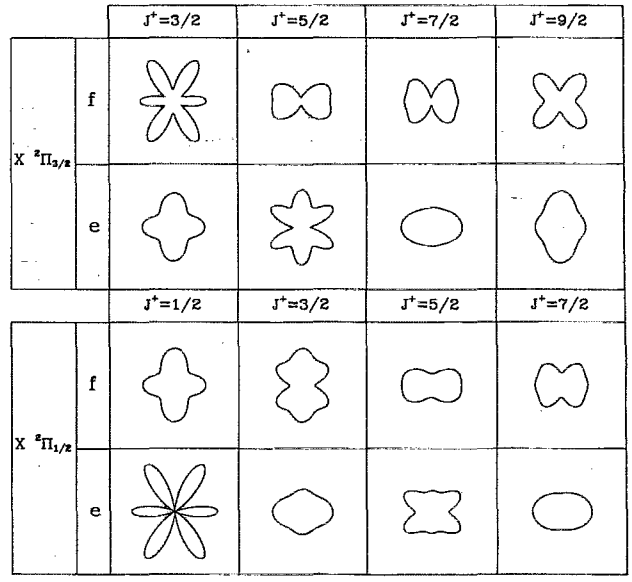

FIG. 5. Photoelectron angular distributions corresponding to the J^+ rotational levels of Fig. 4. Terms up to β_6 are included and 0° is vertical.

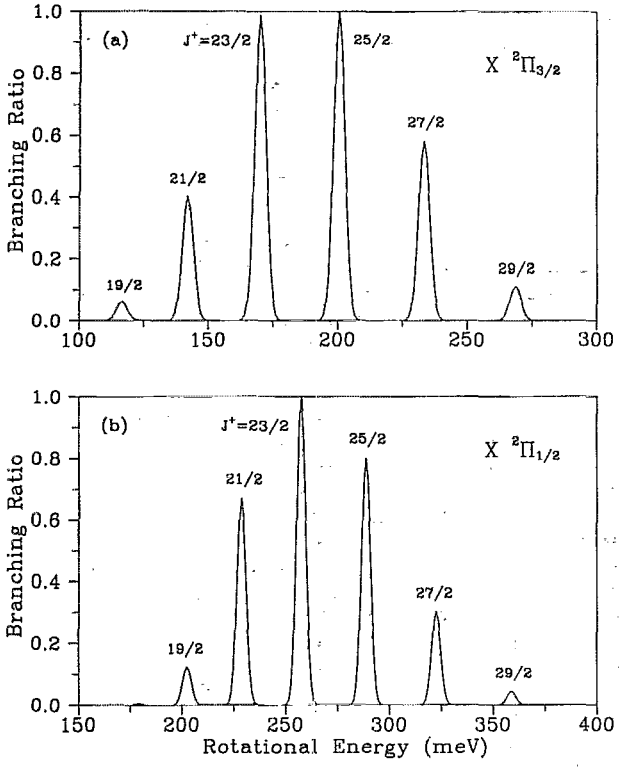

FIG. 6. Rotational ion distributions resulting from (2 + 1) REMPI via the $S(10)$ branch of the $F\,^1\Delta_2$ Rydberg state of HCl. The photoelectron energy is about 1.45 eV. The spectra are convoluted with a Gaussian detector function with an FWHM of 5 meV. A sum over the (+) and (−) parity components of the J^+ levels is assumed.

vored in the (−) parity component (solid bar) of each rotational state. The same behavior is also seen in the case of HBr.[13-15] About 18% population (20% for HBr) is predicted to occur in the (+) parity component (cross-hatched bar) in both spin-orbit states. Further decomposition shows that about 41.3% of the total ion population arises from s-wave contributions, 2.4% from p wave, 40.5% from d wave, 15.2% from f wave, and 0.6% from higher waves. This distribution reflects the angular momentum composition of the photoelectron matrix element. The magnitudes, $|D_l^{(-)}|$, of the incoming-wave normalized partial-wave dipole amplitude at the photoelectron energy of 50 meV are 0.1813, 0.0128, 0.1283, 0.0462, and 0.0110 for $l = 0$–4, respectively, in the $k\sigma$ channel; 0.0719, 0.1330, 0.0814, and 0.0173, for $l = 1$–4, respectively, in the $k\pi$ channel; and 0.0995, 0.0881, and 0.0166 for $l = 2$–4, respectively, in the $k\delta$ channel. Whereas the $3\pi \rightarrow k\pi$ and $3\pi \rightarrow k\delta$ channels contribute about equally to the (+) parity component of J^+ levels in HCl, the $5\pi \rightarrow k\delta$ channel in the photoionization of HBr is responsible for most of the population in the (+) parity component.

Figure 5 shows rotationally resolved photoelectron angular distributions for the parity components of the J^+ rotational levels for both spin-orbit ionic states (see Fig. 4). Contributions from high-l partial waves are evident, especially for the (+) parity component of lower J^+ levels. Again, based on the parity-selection rule of Eq. (4), only even or odd partial waves contribute to the photoelectron angular distributions of a specific parity component of an ion rotational level. Note that the photoelectron angular distributions for the $X\,^2\Pi_{1/2}$ spin-orbit state shown in Fig. 5 are similar to those for (2 + 1′) REMPI of HBr via the $S(0)$ branch of the $F\,^1\Delta_2$ state.[15] Note also that the photoelectron angular distributions of Figs. 2 and 5 are plotted assuming $\beta_0 = 1$ and the polarization vector is vertical ($\theta = 0°$).

B. (2+1) REMPI via the $F\,^1\Delta_2$ Rydberg state

Figure 6 shows the rotational ion distributions resulting from one-color (2 + 1) REMPI via the $S(10)$ branch of the $F\,^1\Delta_2$ Rydberg state of HCl. The photoelectron energy is about 1.45 eV. These spectra are convoluted with a Gaussian detector function with an FWHM of 5 meV. A sum over (+) and (−) parity components is assumed. In these distributions the high-J limit has been reached. These spectra clearly differ from those of low-J transitions. For example, $\Delta N = 0$ and 1 transitions are predicted to be equally intense for the $X\,^2\Pi_{3/2}$ ion in contrast to the intense $\Delta N = 0$ transition observed for the $S(0)$ branch of the $F\,^1\Delta_2$ state (cf. Figs. 1 and 6). Figure 7 shows the rotationally resolved photoelectron angular distributions associated with the ion distributions of Fig. 6. An incoherent sum over (+) and (−) parity components is assumed. Clearly, the underlying partial-wave composition of the angular distributions for the most-intense peaks ($J^+ = 23/2$ and 25/2) of the $X\,^2\Pi_{3/2}$ ion are quite different (e.g., more d wave for $J^+ = 25/2$). Note that both even and odd partial waves contribute to these distributions due to the parity-selection rule of Eq. (4). To provide further insight into the photoionization dynamics and to compare with the results of the studies of HBr, we present rotational ion distributions for the parity components of the Λ doublet of the ionic rotational levels in Fig. 8.

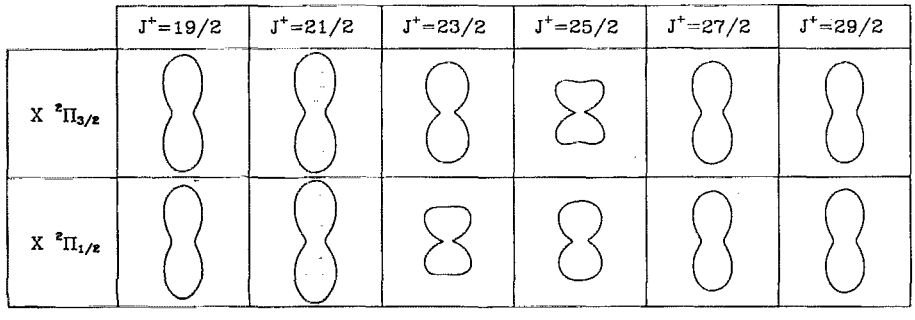

FIG. 7. Photoelectron angular distributions corresponding to the J^+ rotational levels of Fig. 6. An incoherent sum over the (+) and (−) parity components of the J^+ levels is assumed. 0° is vertical.

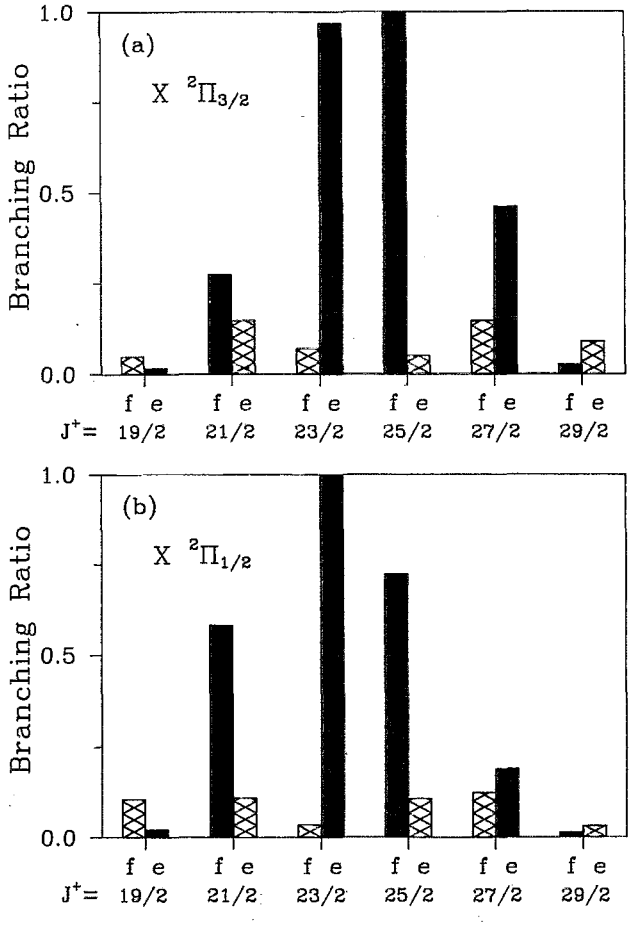

FIG. 8. Rotational ion distributions for the parity components of the J^+ levels associated with Fig. 6.

As seen in the cases of HBr and HCl in the lower J transitions, about 17% population is predicted in the (+) component (cross-hatched bar) of the ionic rotational levels. The physical origin of this distribution has been discussed earlier. A similar distribution for the $X\,^2\Pi_{1/2}$ ion is also seen in HBr in the high-J limit.

ACKNOWLEDGMENTS

This work was supported by grants from the National Science Foundation, Air Force Office of Scientific Research, and the Office of Health and Environmental Research of the U. S. Department of Energy. We also acknowledge use of resources of the Jet Propulsion Laboratory /Caltech Cray X-MP/18 Supercomputer.

[1] R. N. Compton and J. C. Miller, in *Laser Applications in Physical Chemistry*, edited by D. K. Evans (Dekker, New York, 1988).
[2] K. Kimura, Int. Rev. Phys. Chem. **6**, 195 (1987).
[3] S. T. Pratt, P. M. Dehmer, and J. L. Dehmer, in *Advances in Multiphoton Processes and Spectroscopy*, edited by S. H. Lin (World Scientific, Singapore, 1988), and the references and tabulations of REMPI-PES studies therein.
[4] W. G. Wilson, K. S. Viswanathan, E. Sekreta, and J. P. Reilly, J. Phys. Chem. **88**, 672 (1984); K. S. Viswanathan, E. Sekreta, E. R. Davidson, and J. P. Reilly, *ibid.* **90**, 5078 (1986); K. S. Viswanathan, E. Sekreta, and J. P. Reilly, *ibid.* **90**, 5658 (1986); X. Song, E. Sekreta, J. P. Reilly, H. Rudolph, and V. McKoy, J. Chem. Phys. **91**, 6062 (1989).
[5] S. W. Allendorf, D. J. Leahy, D. C. Jacobs, and R. N. Zare, J. Chem. Phys. **91**, 2216 (1989).
[6] E. F. McCormack, S. T. Pratt, J. L. Dehmer, and P. M. Dehmer, J. Chem. Phys. **92**, 4734 (1990); M. A. O'Halloran, S. T. Pratt, P. M. Dehmer, and J. L. Dehmer, *ibid.* **87**, 3288 (1987); M. A. O'Halloran, P. M. Dehmer, S. T. Pratt, J. L. Dehmer, and F. S. Tomkins, *ibid.* **90**, 930 (1989).
[7] S. T. Pratt, P. M. Dehmer, and J. L. Dehmer, J. Chem. Phys. **92**, 262 (1990).
[8] E. de Beer, C. A. de Lange, J. A. Stephens, K. Wang, and V. McKoy, J. Chem. Phys. **95**, 714 (1991).
[9] K. Müller-Dethlefs, M. Sander, and E. W. Schlag, Chem. Phys. Lett. **112**, 291 (1984).
[10] M. Sander, L. A. Chewter, K. Müller-Dethlefs, and E. W. Schlag, Phys. Rev. A **36**, 4543 (1987).
[11] M. Braunstein, V. McKoy, S. N. Dixit, R. G. Tonkyn, and M. G. White, J. Chem. Phys. **93**, 5345 (1990).
[12] K. S. Haber, Y. Jiang, G. Bryant, H. Lefebvre-Brion, and E. R. Grant, Phys. Rev. A (in press).
[13] J. Xie and R. N. Zare, Chem. Phys. Lett. **159**, 399 (1989).
[14] J. Xie and R. N. Zare (private communication).
[15] K. Wang and V. McKoy, J. Chem. Phys. (in press).
[16] J. M. Brown, J. T. Hougen, K.-P. Huber, J. W. C. Johns, I. Kopp, H. Lefebvre-Brion, A. J. Merer, D. A. Ramsay, J. Rostas, and R. N. Zare, J. Mol. Spectrosc. **55**, 500 (1975).
[17] K. Wang and V. McKoy, J. Chem. Phys. **95**, 4977 (1991).
[18] J. Xie and R. N. Zare, J. Chem. Phys. **93**, 3033 (1990).
[19] S. N. Dixit and V. McKoy, Chem. Phys. Lett. **128**, 49 (1986).
[20] G. Raseev and N. Cherepkov, Phys. Rev. A **42**, 3948 (1990).
[21] R. R. Lucchese, G. Raseev, and V. McKoy, Phys. Rev. A **25**, 2572 (1982).
[22] R. R. Lucchese, K. Takatsuka, and V. McKoy, Phys. Rep. **131**, 147 (1986).
[23] W. J. Hunt and W. A. Goddard, Chem. Phys. Lett. **3**, 414 (1969).
[24] T. H. Dunning, Jr., Chem. Phys. Lett. **7**, 423 (1970).
[25] T. H. Dunning, Jr., J. Chem. Phys. **53**, 2823 (1970); **55**, 3958 (1971).